IEEE Access
Multidisciplinary | Rapid Review | Open Access Journal

Received March 27, 2021, accepted April 9, 2021, date of publication April 15, 2021, date of current version April 29, 2021.

Digital Object Identifier 10.1109/ACCESS.2021.3073592

Kriging Aerodynamic Modeling and Multi-Objective Control Allocation for Flying Wing UAVs With Morphing Trailing-Edge

XINHUI ZHAO[1,2], YANPING YANG[1], AND XIAOPING MA[1]
[1]Institute of Engineering Thermophysics, Chinese Academy of Sciences, Beijing 100190, China
[2]University of Chinese Academy of Sciences, Beijing 100049, China

Corresponding author: Yanping Yang (yanping-yang@qq.com)

This work was supported in part by the National Natural Science Foundation of China under Grant 61901448, Grant 61871401, and Grant 12002340.

ABSTRACT Flexible skin and continuous deformable control surface are the basic of adaptive wing technology for future aircraft. This paper presents a continuous morphing trailing-edge and its control allocation method for the flying wing Unmanned Aerial Vehicle (UAV). Firstly, we apply the Kriging method to establish the aerodynamic model of the morphing trailing-edge, with the initial sample points generated by the non-uniform optimal Latin Hypercube Sampling (LHS). Then, based on the Kriging model, the multi-objective control allocation problem is converted into a standard optimization form. To solve such problem, we design a Comprehensive Multi-Objective Particle Swarm Optimization (C-MOPSO) algorithm and an improved Hierarchical MOPSO (H-MOPSO) algorithm, in which multiple optimization objectives are prioritized and hierarchically optimized using the PSO algorithm. As for performance analysis, an attitude angle tracking flight control system is established to validate the effectiveness of our proposed control allocation methods. Simulation results show that both the C-MOPSO and H-MOPSO methods have similar performance in attitude angle tracking, while H-MOPSO achieves better multi-objective allocation performance.

INDEX TERMS Flying wing UAV, morphing trailing-edge, Kriging aerodynamic modeling, multi-objective control allocation, particle swarm optimization.

I. INTRODUCTION

Compared with conventional UAVs, flying wing UAVs adopt the blended-wing-body configuration and eliminate the empennage, therefore, they have more advantages in aerodynamic, structural and stealth performance, such as an extremely low radar cross-section (RCS) and a significant reduction in fuel consumption and aerodynamic noise [1], [2]. These benefits make the flying wing UAV a popular research direction in both military and civil fields [3], [4]. However, due to the lack of vertical and horizontal stabilizers, the stability and control efficiency of flying wing UAVs are particularly prominent issues. Additionally, the gaps between the discrete control surfaces further weaken the control efficiency, adversely affect the stealth performance, and increase the overall drag of the aircraft.

The associate editor coordinating the review of this manuscript and approving it for publication was Sotirios Goudos.

To improve the aerodynamic performance of flying wing UAVs with conventional control surfaces, a continuous deformable control surface (namely, *morphing control surface*) is proposed, which can smoothly change the airfoil profile along the span. Such design can be attained through morphing wing technologies, which is a promising technique in innovative adaptive structures and can be commonly classified into two types: airfoil-level morphing wing and wing-level morphing wing [5], [6] (see Fig.1).

Among various morphing wing schemes, camber morphing wings have better control performance and higher aerodynamic efficiency. Explicitly, a camber morphing wing can alter the lift distribution along the wing by changing the camber along the spanwise direction, so that the aerodynamic forces and moments can be adapted to the desired control commands. Trailing-edge having continuous deformable structure, namely *morphing trailing-edge*, is one of the simplest and most effective methods for realizing camber

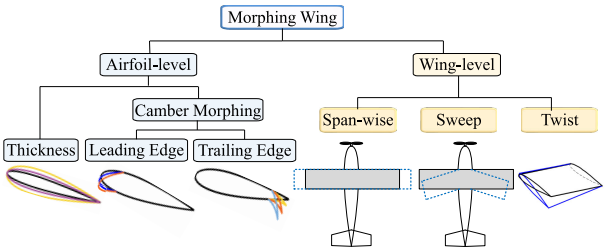

FIGURE 1. Classification of morphing wing technologies.

morphing. Since the trailing-edge region has high aerodynamic and structural effectiveness, we focus camber morphing research on this region.

The existing research on camber morphing mainly concentrates on intelligent materials, flexible structures and advanced actuators. In terms of control, the main objective is to reach the specific camber to adapt to the current flight phase. In the current researches, Wang *et al.* investigated the control problem of morphing wings based on switched nonlinear systems and adaptive dynamic programming [7]. The author of [8] systematically studied the control authority of camber morphing flying wings. The main challenge in the design of the control system for flying wing UAVs with camber morphing is the control redundancy and multi-axis coupling. To solve this problem, control allocation is developed.

Control allocation is an effective approach for solving the control redundancy caused by multiple control surfaces and unconventional surfaces. Current control allocation methods, such as direct allocation, pseudoinverse, daisy chaining and error minimization using linear programming, are based on the assumption that the aerodynamic control forces and moments are linear functions of control surface deflections [9]. However, for most advanced aircraft, such assumption is not accurate, and the error caused by this assumption is usually mitigated by the robustness of the feedback control law, which further increases the burden of the flight control system. To improve the accuracy of control allocation, nonlinear control allocation methods are proposed.

In nonlinear control allocation, the nonlinear aerodynamic model is usually established by polynomials, piecewise linear functions or nonlinear correction terms [10]–[12]. These methods are relatively simple and practical, but it is difficult to fit complex nonlinear aerodynamic characteristics. Specifically, the aerodynamic characteristics of the morphing trailing-edge flying wing UAV not only exhibit strong nonlinearity but also have the problem of control actuator interactions. Therefore, conventional aerodynamic modeling methods are difficult to meet the design requirements. Considering the specific aerodynamic characteristics, using the Kriging algorithm to establish the aerodynamic model is a very targeted solution. Generally, the Kriging model is accurate for nonlinear approximation, and it is easier to deal with multi-dimensional input-output aerodynamic data [13]–[16]. Therefore, in this paper, we determine the aerodynamic data sample points by the Design of Experiment (DoE) and establish the aerodynamic model using the *ordinary Kriging* algorithm.

For the control allocation problem formulated by the Kriging aerodynamic model, the traditional mathematical programming method is not applicable because the Kriging aerodynamic model is a surrogate model. Therefore, we need to find new control allocation methods. To the best of our knowledge, it is good to exploit Comprehensive Multi-Objective Particle Swarm Optimization (C-MOPSO) and to design an improved Hierarchical MOPSO algorithm (H-MOPSO). Both methods can handlethe multiple optimization objectives well and perform optimization by applying the Particle Swarm Optimization (PSO) algorithm.

Considering the above rationale, this paper aims to provide solutions to the above design, and the main contributions of this paper can be summarized as follows:

(1) A continuously morphing trailing-edge control surface is designed for a flying wing UAV. The control performance is improved by increasing the degree of freedom of the control surface.
(2) The Kriging algorithm is innovatively adopted to establish the aerodynamic model of morphing trailing-edge and to solve the control allocation problem. Specifically, an improved nonuniform optimal Latin hypercube sampling method is designed to generate the initial sample points for modeling.
(3) We design two effective and heuristic algorithms specifically for the control allocation problem based on Kriging aerodynamic modeling, namely, C-MOPSO and H-MOPSO. Both algorithms are PSO-based methods to solve the multi-objective optimization, in which C-MOPSO has advantages in algorithm efficiency and realizability, but the result may not be optimal. H-MOPSO is based on the priority ranking of multiple objectives, which can achieve a trade-off between multiple objectives and achieve better performance.

The remainder of this paper is structured as follows. The concept and design of the morphing trailing-edge are presented in Section II. The DoE and Kriging aerodynamic modeling methods are provided in Section III. In Section IV, we design the C-MOPSO and H-MOPSO algorithms to solve the multi-objective control allocation problem, with the validation of the proposed methods by flight control simulation evaluated in Section V. Finally, the concluding remarks are summarized in Section VI.

II. MORPHING TRAILING-EDGE FLYING WING UAV

Two basic configurations of morphing trailing-edge are presented in Fig. 2:

(1) Chordwise morphing trailing-edge (Fig. 2.(a))
By curving the trailing-edge along chordwise, it would allow the wing to achieve near-optimal profiles smoothly under different flight phases, thus leading to an enhanced aerodynamic performance.

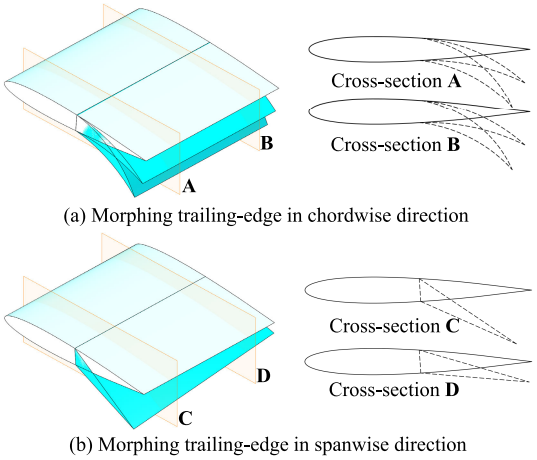

(a) Morphing trailing-edge in chordwise direction

(b) Morphing trailing-edge in spanwise direction

FIGURE 2. Two morphing trailing-edge configurations.

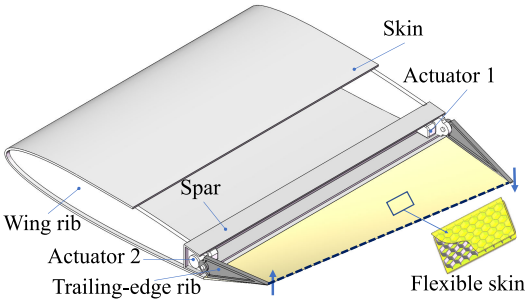

FIGURE 3. Sketch of a morphing trailing-edge wing structure design scheme.

(2) Spanwise morphing trailing-edge (Fig. 2.(b))
By twisting the trailing-edge along spanwise, the lift distribution along the span of the wing can be manipulated, which can enhance the flight performance and the control authority of the UAV. This structure is the basis of the following study. Based on this configuration, it is assumed that the morphing trailing-edge only twists along the span direction, and there is no flexible deformation along the chordwise direction.

To achieve the morphing configuration shown in Fig.2 (b), we designed a morphing trailing-edge structure, as shown in Fig.3. The actuator 1 and actuator 2 are installed on the left and right ends of the wing to control the external shape of the morphing trailing-edge. Conventional rigid skin is laid on the main wing, and flexible skin is laid on the trailing-edge. The flexible skin comprising a cellular honeycomb core covered with a compliant face-sheet. The function of the face-sheet is to provide a smooth aerodynamic surface. The flexible cellular core supports the face-sheet and provides the required out-of-plane stiffness of the composite skin [17]. When the deflections of actuator 1 and actuator 2 are different, the flexible skin deforms continuously along the wingspan direction without gaps.

Based on above designs and inspirations, the flying wing UAV presented in this paper is shown in Fig. 4, and the main parameters of this UAV are listed in Table. 1. By applying

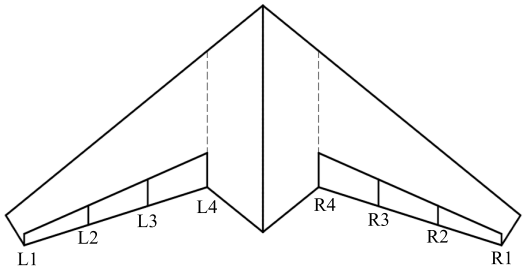

FIGURE 4. Flying wing UAV and actuators layout.

TABLE 1. Main parameters of the flying wing UAV.

Parameter	Notation	Value
Wing span	b	1.2m
Body length	l	0.5m
Wing area	S_{ref}	0.24m^2
Mean aero chord	MAC	0.275m
Sweepback angle	Λ	38°
Cruise speed	Vc	50m/s

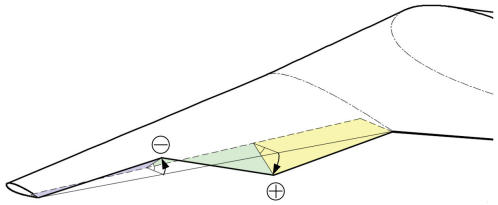

FIGURE 5. Deflection of trailing-edge.

the morphing wing technology, the trailing-edge of the flying wing UAV can be continuous and without gaps. Actuators are set at L1, L2, $\cdots$, and R4 (see Fig. 4) to control the deflection of the trailing-edge, and the deflection range is limited to $[-30°, +30°]$, with the upward deflection being negative and the downward deflection being positive (see Fig. 5).

III. KRIGING AERODYNAMIC MODELING

Considering the nonlinear and coupling characteristics, we utilized Kriging algorithm to establish the aerodynamic model of the morphing trailing-edge.

A. DESIGN OF EXPERIMENT

The first step in establishing the Kriging model is to choose the initial sample points by using the design of experiment (DoE) method. To obtain a set of initial sample points that satisfies both the projection uniformity and the spatial uniformity, optimal Latin hypercube sampling (OLHS) with the maximin criterion was developed and is widely applied in Kriging modeling [18], [19].

However, as the aerodynamic characteristics of the morphing trailing-edge do not vary uniformly in the design space, it is not reasonable to sample points uniformly in the design space. Specifically, for small control surface deflection, the aerodynamic data have an approximate linear characteristic, and the aerodynamic nonlinearity is obvious at large control surface deflection. Therefore, based on the OLHS method, it is reasonable to select the sample points

by the non-uniform division method (namely, non-uniform OLHS). More explicitly, the algorithm samples sparse points in a small control surface deflection range and samples dense points in a large deflection range.

In the conceptual design stage, the key point is to quickly analyze the design feasibility and the gains, and low-fidelity aerodynamic analysis methods are usually utilized. According to the selected initial sample points, we choose the three-dimensional (3D) panel method to evaluate the aerodynamic characteristics of the morphing trailing-edge flying wing UAV under various actuator deflections. The 3D panel method is an aerodynamic analysis tool with high computational efficiency, and has sufficient accuracy to evaluate the trends of aerodynamic coefficients [8]. Specifically, we choose XFLR5 software[1] embedded with 3D panel method as the aerodynamic analysis tool. For each morphing trailing-edge configuration determined by the DoE, the corresponding 3D shape model of the flying wing UAV is established in XFLR5, while the 3D panel method is used to quickly obtain the aerodynamic parameters.

B. KRIGING AERODYNAMIC MODELING

The *ordinary Kriging* (*Kriging* for short) model used in this context can approximate highly nonlinear functions and provide error prediction, which is very useful for surrogate model management. The Kriging model is a spatial interpolation model that is composed of a regression model and stochastic process. In this model, the aerodynamic function C_x is expressed as [20]

$$C_x(\mathbf{x}) = m + Z(\mathbf{x}), \tag{1}$$

where C_x represent aerodynamic coefficient, $\mathbf{x} = [\boldsymbol{\delta}, \alpha, \beta, Ma]^{\mathrm{T}}$ is the input vector, representing actuator deflections, angle of attack, sideslip angle and Mach number, respectively. m is a constant global regression model, and $Z(\mathbf{x})$ is a stationary Gaussian random function used to calibrate the local deviation of the global regression model. For n_s sample points, the covariance matrix of $Z(\mathbf{x})$ is given by (2)

$$\mathrm{Cov}\left[Z(\mathbf{x}^i), Z(\mathbf{x}^j)\right] = \sigma^2 \mathbf{R}\left[r\left(\mathbf{x}^i, \mathbf{x}^j\right)\right] \quad i, j = 1, \cdots, n_s, \tag{2}$$

in which σ^2 is the variance in $Z(\mathbf{x})$; $\mathbf{R}$ is an $n_s \times n_s$ symmetric correlation matrix, and $r\left(\mathbf{x}^i, \mathbf{x}^j\right)$ is a correlation function between any two sample points $\mathbf{x}^i$ and $\mathbf{x}^j$. A pervasive correlation function is the Gauss correlation function, which is defined as

$$r\left(\mathbf{x}^i, \mathbf{x}^j\right) = \prod_{k=1}^{n} \exp\left(-\theta_k \left\|\mathbf{x}_k^i - \mathbf{x}_k^j\right\|^2\right), \tag{3}$$

where θ_k is a correlation parameter that denotes the importance of factor k and n is the number of design variables.

[1]In the concept and preliminary design stage of aircraft technology, XFLR5 software is convenient and efficient in calculating the aerodynamic characteristics of morphing wings, and has been adopted by many researches [5].

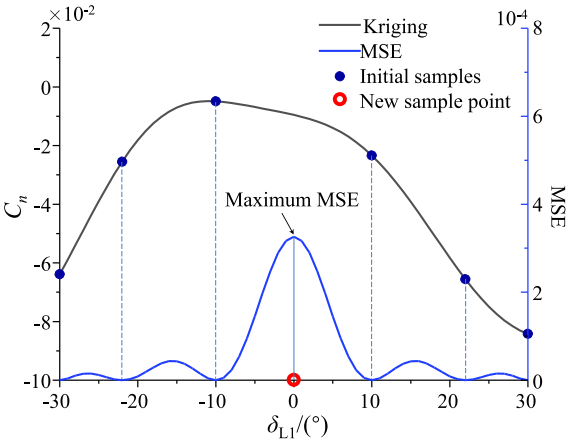

FIGURE 6. Schematic diagram of the MSE infill-sampling criterion.

Given a set of n_s responses $\mathbf{Y} = [C_x(\mathbf{x}^1), \cdots C_x(\mathbf{x}^{n_s})]^{\mathrm{T}}$, the predicted value $\hat{C}_x$ at an untried value of $\mathbf{x}^0$ is

$$\hat{C}_x\left(\mathbf{x}^0\right) = \hat{m} + \mathbf{r}^{\mathrm{T}}\mathbf{R}^{-1}\left(\mathbf{Y} - \hat{m}\mathbf{1}\right), \tag{4}$$

in which $\hat{m}$ is the maximum likelihood estimator of the mean of the random field and is given by (5); $\mathbf{r}$ is an $n \times 1$ vector of correlation functions (shown in (6)), and $\mathbf{1}$ is an n-dimensional unit vector.

$$\hat{m} = \left(\mathbf{1}^{\mathrm{T}}\mathbf{R}^{-1}\mathbf{1}\right)^{-1}\mathbf{1}^{\mathrm{T}}\mathbf{R}^{-1}\mathbf{Y}, \tag{5}$$

$$\mathbf{r} = \left[r\left(\mathbf{x}^0, \mathbf{x}^1\right), r\left(\mathbf{x}^0, \mathbf{x}^2\right), \cdots r\left(\mathbf{x}^0, \mathbf{x}^{n_s}\right)\right]^{\mathrm{T}}. \tag{6}$$

By constructing the Kriging surrogate model, we can obtain the continuous function of the aerodynamic coefficient varying with the actuator deflection angles.

C. INFILL CRITERIA

To improve the computational efficiency, the initial sample points obtained by the DoE are relatively small; thus, the accuracy of the initial Kriging aerodynamic model may not meet the design requirement. To improve the accuracy, we need to add some new sample points generated by the infill criteria to the initial Kriging model. The infill criterion adopted in this paper is the mean square error (MSE) infill-sampling criterion, which can effectively improve the global precision of the Kriging model [21], [22]. The main idea of the MSE criterion is that the point with the maximum mean squared error in the design space is infilled into the Kriging model.

In the Kriging model, the accuracy of the prediction value largely depends on the distance from the sample points and the MSE of the predictor at $\mathbf{x}$ as follows:

$$s^2(\mathbf{x}) = \hat{\sigma}^2\left[1 - \mathbf{r}^{\mathrm{T}}\mathbf{R}^{-1}\mathbf{r} + \frac{\left(1 - \mathbf{1}\mathbf{R}^{-1}\mathbf{r}\right)^2}{\mathbf{1}^{\mathrm{T}}\mathbf{R}^{-1}\mathbf{1}}\right], \tag{7}$$

where $\hat{\sigma}^2$ is the estimated value of the variance in Z given by:

$$\hat{\sigma}^2 = \frac{(\mathbf{Y} - \mathbf{1}\hat{m})^{\mathrm{T}}\mathbf{R}^{-1}(\mathbf{Y} - \mathbf{1}\hat{m})}{n_s}. \tag{8}$$

TABLE 2. Four morphing trailing-edge configurations for accuracy verification.

No.	δ_{L1}	δ_{L2}	δ_{L3}	δ_{L4}
1	30°	30°	30°	30°
2	0°	20°	-20°	0°
3	20°	20°	-20°	-20°
4	-30°	-30°	-30°	-30°

By solving the optimization problem in (9), we can obtain a new sample point. Fig. 6 is the schematic diagram of the MSE infill-sampling criterion. The red dot is the new sample point after the actual calculation. This infilling sampling process is executed until $s^2_{\max} \leq 10^{-4}$.

$$\begin{aligned} &\text{maximize } s^2(\mathbf{x}) \\ &\text{subject to } \mathbf{x} \in [\mathbf{x}_{\min}, \mathbf{x}_{\max}]. \end{aligned} \tag{9}$$

To verify the accuracy of the Kriging aerodynamic model, four morphing trailing-edge configurations are selected from the nonsample point set (refer to Table. 2), and the aerodynamic data predicted by the Kriging aerodynamic model are compared with the value calculated by the 3D panel method (shown in Fig. 6). Fig. 6 shows that the Kriging aerodynamic model can accurately predict aerodynamic characteristics.

IV. MULTI-OBJECTIVE CONTROL ALLOCATION METHOD

A. FORMULATION OF MULTI-OBJECTIVE CONTROL ALLOCATION

Using a morphing trailing-edge as a control surface often leads to control coupling and redundancy. *Control coupling* means that any actuator deflection may simultaneously generate roll, pitch and yaw moments. *Redundancy* refers to the fact that multiple combinations of actuator deflection can produce the same desired moments. To solve the control challenges, we introduce control allocation and distribute the control requirements to each actuator. The structure of the flight control system, including control allocation, is shown in Fig. 8.

Typically, for the control allocation problem, it is assumed that there is a linear relationship between the control-induced moments and the control actuator displacements; hence, the linear control allocation problem of traditional multicontrol surfaces is defined as

$$\mathbf{v}(t) = \mathbf{B}\mathbf{u}(t) \quad \begin{cases} \mathbf{u}_{\min} \leq \mathbf{u} \leq \mathbf{u}_{\max} \\ \dot{\mathbf{u}}_{\min} \leq \dot{\mathbf{u}} \leq \dot{\mathbf{u}}_{\max}, \end{cases} \tag{10}$$

where $\mathbf{v}(t) \in \mathbb{R}^m$ is the desired virtual control vector calculated by the flight control law and is generally set as $\mathbf{v}(t) = [C_{l\,\mathrm{des}}(t), C_{m\,\mathrm{des}}(t), C_{n\,\mathrm{des}}(t)]^{\mathrm{T}}$. $\mathbf{u}(t) \in \mathbb{R}^n$ is the actual control input vector, and $\dot{\mathbf{u}}$ denotes the deflection rate vector of the actuators. $\mathbf{B} \in \mathbb{R}^{m\times n}$ is the control efficiency matrix defined by the Jacobian

$$\mathbf{B} = \begin{bmatrix} \frac{\partial C_{l-\delta_1}}{\partial \delta_1} & \frac{\partial C_{l-\delta_2}}{\partial \delta_2} & \cdots & \frac{\partial C_{l-\delta_n}}{\partial \delta_n} \\ \frac{\partial C_{m-\delta_1}}{\partial \delta_1} & \frac{\partial C_{m-\delta_2}}{\partial \delta_2} & \cdots & \frac{\partial C_{m-\delta_n}}{\partial \delta_1} \\ \frac{\partial C_{n-\delta_1}}{\partial \delta_1} & \frac{\partial C_{n-\delta_2}}{\partial \delta_2} & \cdots & \frac{\partial C_{n-\delta_n}}{\partial \delta_n} \end{bmatrix}, \tag{11}$$

where $C_{l-\delta_1}$ represents the roll moment coefficient caused by the actuator deflection δ_1.

However, for the morphing trailing-edge flying wing UAV, the forces and moments generated by the control surfaces are almost always nonlinear functions of actuator displacement. Therefore, the control allocation results based on (10) are inaccurate and need to be improved. In this paper, the mapping relationship among the actuator deflections to the control aerodynamic forces and the moments are established by the Kriging method. Then, the control allocation problem is formulated as follows:

$$\mathbf{v}(t) = \mathbf{f}[\mathbf{u}(t)] \quad \begin{cases} \mathbf{u}_{\min} \leq \mathbf{u} \leq \mathbf{u}_{\max} \\ \dot{\mathbf{u}}_{\min} \leq \dot{\mathbf{u}} \leq \dot{\mathbf{u}}_{\max}, \end{cases} \tag{12}$$

where $\mathbf{f}$ modeled by the Kriging method represents the mapping between the desired virtual control vector and the actuator deflections. To obtain an appropriate solution to (12), this control allocation problem is transformed into an optimization problem, and then (12) can be re-expressed as the optimization problem with minimum allocation errors, as given by:

$$\begin{aligned} &\text{minimize } J_0(\mathbf{u}) = \|\mathbf{v}(\mathbf{t}) - \mathbf{f}[\mathbf{u}(\mathbf{t})]\| \\ &\text{subject to } \begin{cases} \mathbf{u}_{\min} \leq \mathbf{u} \leq \mathbf{u}_{\max} \\ \dot{\mathbf{u}}_{\min} \leq \dot{\mathbf{u}} \leq \dot{\mathbf{u}}_{\max}. \end{cases} \end{aligned} \tag{13}$$

In addition to the minimum allocation errors, the control allocation also needs to consider the lift, drag and energy cost of actuator deflections. More explicitly, during the climbing and maneuver phases, an increase in lift and a reduction in drag are needed as much as possible. During the cruise phase, the energy costs of actuator deflections and drag need to be reduced. For the landing phase, increased lift is necessary to prevent collisions, and increased drag helps to slow down. Through the above analysis, the control allocation problem is a multi-objective optimization problem, and the additional optimization objectives have the following candidates:

$$\begin{cases} J_1(\mathbf{u}) = ||\mathbf{u} - \mathbf{u}_0|| \\ J_2(\mathbf{u}) = C_L(\mathbf{u}) \\ J_3(\mathbf{u}) = C_D(\mathbf{u}), \end{cases} \tag{14}$$

where J_1, J_2 and J_3 represent the energy cost of actuator deflections, lift and drag objectives, respectively. $\mathbf{u}_0$ is the previous control input vector. Finally, the multi-objective control allocation problem can be expressed in the following form:

$$\begin{aligned} &\text{minimize } F(\mathbf{u}) = [J_0(\mathbf{u}), J_1(\mathbf{u}), J_2(\mathbf{u}), J_3(\mathbf{u})] \\ &\text{subject to } \begin{cases} \mathbf{u}_{\min} \leq \mathbf{u} \leq \mathbf{u}_{\max} \\ \dot{\mathbf{u}}_{\min} \leq \dot{\mathbf{u}} \leq \dot{\mathbf{u}}_{\max}. \end{cases} \end{aligned} \tag{15}$$

B. COMPREHENSIVE MOPSO

We apply the multi-objective particle swarm optimization (MOPSO) algorithm to solve the multi-objective control allocation problem in (15). The MOPSO algorithm is

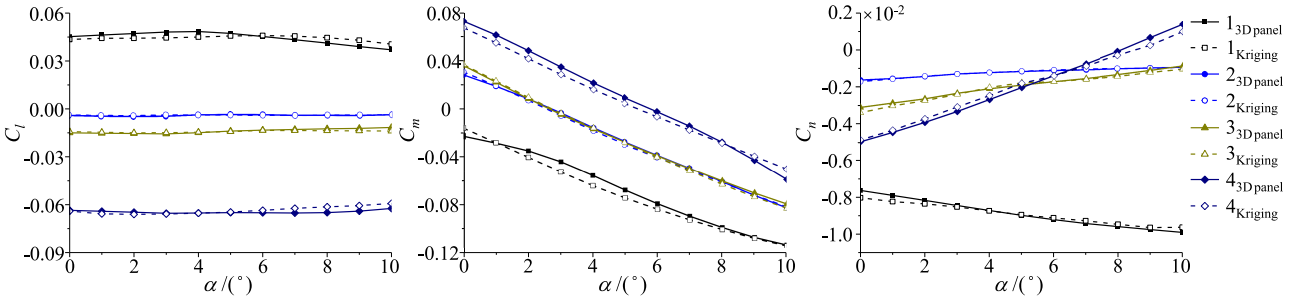

FIGURE 7. Comparison of the Kriging model and 3D panel method calculation results.

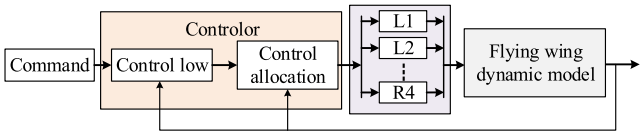

FIGURE 8. Flight control system architecture.

a multiple objective heuristic optimization method derived from the single-objective particle swarm optimization (PSO) algorithm. It has the advantages of simple calculation, less dependence on the set of initial points, fast convergence, easy implementation, and small influence of parameters on the solution [23].

To solve the multi-objective optimization problem in (15), we design a comprehensive MOPSO (C-MOPSO) method based on the comprehensive performance index for different allocation objectives. In the C-MOPSO, multiple allocation objectives are combined into a single objective using a set of weights, and the multi-objective control allocation problem can be expressed as

$$\begin{aligned} &\text{minimize } G(\mathbf{u}) = \kappa J_0(\mathbf{u}) + w_1 J_1(\mathbf{u}) + w_2 J_2(\mathbf{u}) + w_3 J_3(\mathbf{u}) \\ &\text{subject to } \begin{cases} \mathbf{u}_{\min} \le \mathbf{u} \le \mathbf{u}_{\max} \\ \dot{\mathbf{u}}_{\min} \le \dot{\mathbf{u}} \le \dot{\mathbf{u}}_{\max}, \end{cases} \end{aligned} \tag{16}$$

where $w_i (i = 1, 2, 3)$ is the weighting factor for the ith optimization objective, and κ is the penalty factor. The analytic hierarchy process (AHP) method is used to determine the weights for each objective [24].

The main advantages of the C-MOPSO method are the simplicity and the low computational cost because the single-objective algorithm does not need to store and handle nondominated solutions. However, the C-MOPSO method relies on expert knowledge to calculate the weights for constructing the comprehensive optimization index. If the weights are not properly set, the optimal result might not be obtained. For this reason, we propose an improved method, namely, the hierarchical MOPSO method.

C. HIERARCHICAL MOPSO

The hierarchical MOPSO (H-MOPSO) algorithm is an improved algorithm based on the Pareto optimal solution set method, which can handle multi-objective optimization

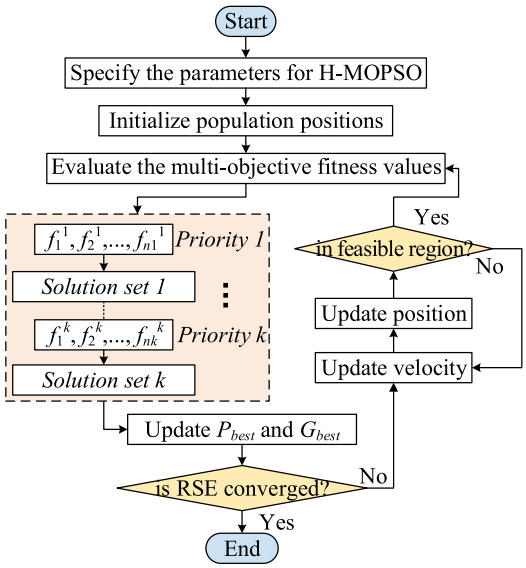

FIGURE 9. The flowchart of H-MOPSO algorithm.

problems according to the different importance of the objectives. The H-MOPSO approach divides multiple optimization objectives into multiple priorities, each of which can have one or more optimization objectives. The optimization sequence is set from high priority to low priority, and the algorithm flowchart is shown in Fig. 9.

The iteration of the proposed H-MOPSO algorithm includes four steps: (1) initialize parameters and population, (2) evaluate particles, (3) update the personal and global best solution ($\mathbf{P}_{best}$ and $\mathbf{G}_{best}$), and (4) update the particle positions.

Step (1): To apply the H-MOPSO, a set of parameters should be set first, which includes the number of particles, the personal and global learning rata, the inertial weight and the termination condition. Table. 3 lists the main parameter settings of H-MOPSO in the context.

The algorithm creates a set of random particle swarms $\mathbf{U}_0 = \{\mathbf{u}_0^1, \mathbf{u}_0^2, \cdots, \mathbf{u}_0^n\}$ in a D-dimensional design space by

$$\mathbf{u}_0^k = \underline{\mathbf{u}} + \text{rand}(\bar{\mathbf{u}} - \underline{\mathbf{u}}) \quad k = 1, \cdots, n, \tag{17}$$

where the subscript of $\mathbf{u}$ represents the number of iterations, and the superscript represents the number of particles in the population. $\bar{\mathbf{u}}$ and $\underline{\mathbf{u}}$ denote the upper and lower bounds on

TABLE 3. Main parameters of MOPSO.

Parameter	Symbol	Value
Dimensions of variables	D	8
Number of particles	n	40
Max iteration	$i_{\max}$	50
Inertia weight range	$[w_{\min}, w_{\max}]$	[0.2,1]
Personal learning rata	c_1	1.2
Global learning rata	c_2	1.2

the actuator deflection, respectively. As we take the position and rate as the constraints of actuators, the deflection range of actuators can be expressed as

$$\begin{cases} \bar{\mathbf{u}} = \min(\mathbf{u}_{\max}, \mathbf{u}_0 + T\dot{\mathbf{u}}_{\max}) \\ \underline{\mathbf{u}} = \max(\mathbf{u}_{\min}, \mathbf{u}_0 + T\dot{\mathbf{u}}_{\min}), \end{cases} \tag{18}$$

where T is the sampling time of the control system.

Step (2): For each particle in the initial population, the multiple objective function fitness values $J_0(\mathbf{u}), \cdots, J_3(\mathbf{u})$ are evaluated by (13) and (14).

Step (3): Based on the multi-objective function fitness values, the $\mathbf{P}_{\text{best}}$ for the ith iteration is decided by

$$\mathbf{P}_{\text{best\_}i} = \begin{cases} \mathbf{u}_i, & \mathbf{u}_i \prec \mathbf{u}_{i-1} \\ \mathbf{u}_{i-1}, & \mathbf{u}_i \succ \mathbf{u}_{i-1} \\ \mathbf{u}_i, & \text{otherwise}, \end{cases} \tag{19}$$

where $\mathbf{u}_i \prec \mathbf{u}_{i-1}$ represents that $\mathbf{u}_i$ dominates $\mathbf{u}_{i-1}$, and vice versa.

To select $\mathbf{G}_{\text{best}}$, multiple objective functions are assigned different priorities according to their importance. For example, in the maneuver phase, minimizing allocation error has the highest priority. The second most important goal is to maximize the lift coefficient and minimize the drag coefficient. Minimizing the energy cost of actuator deflections is relatively unimportant. Therefore, the optimization objective functions can be divided into three levels.

* **Priority 1:** minimizing allocation error J_0;
* **Priority 2:** maximize lift J_1, minimum drag J_2;
* **Priority 3:** minimizing control energy cost J_3.

For the first level (**Priority 1**), there is only one objective J_0, the optimal particle and the particles in this adjacent domain are selected as the *Solution Set* 1, and the radius of the adjacent domain is 20% of the optimal solution. Then, for the second level (**Priority 2**), considering that there are two optimization objectives (J_1 and J_2), we select *Solution Set* 2 from *Solution Set* 1 based on the Pareto method. Specifically, we propose a loose Pareto set (LPS) method, which consists of the Pareto front and points closer to the Pareto front. This approach can improve the diversity of the solutions for the next level. Taking a priority containing two optimization objectives as an example, the schematic diagram of the LPS is shown in Fig. 10. Finally, for the third level (**Priority 3**), there is only one objective J_3, and the optimal particle is selected as the global best solution $\mathbf{G}_{\text{best\_}i}$ for the ith iteration.

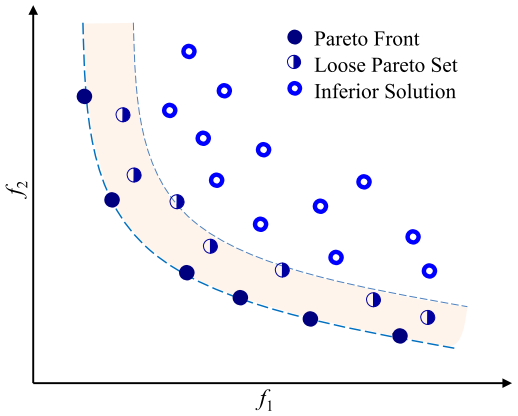

FIGURE 10. The schematic diagram of the loose Pareto set.

Step (4) of the H-MOPSO algorithm is to update the particle position $\mathbf{u_{i+1}}$ the velocity vector $\mathbf{V}_{i+1}$

$$\begin{aligned} \mathbf{u}_{i+1} &= \mathbf{u}_i + \mathbf{V}_{i+1}, \quad i = 1, 2, \cdots, i_{\max} \\ \mathbf{V}_{i+1} &= w \cdot \mathbf{V}_i + c_1 r_1 (\mathbf{P}_{\text{best}-i} - \mathbf{u}_i) \\ &\quad + c_2 r_2 (\mathbf{G}_{\text{best}-i} - \mathbf{u}_i), \end{aligned} \tag{20}$$

where w is the inertial weight used to improve the calculation speed and the quality, $w \in [w_{\min}, w_{\max}]$ (refer to (21)). c_1 is the cognition learning rate, and c_2 is the social learning rate. r_1 and r_2 are the random number in [0, 1].

$$w = w_{\max} - \frac{i \cdot (w_{\max} - w_{\min})}{i_{\max}}. \tag{21}$$

The H-MOPSO algorithm updates the positions of each particle through iteration until the termination conditions are met. The whole H-MOPSO algorithm in pseudocode form is provided in **Algorithm 1**.

V. SIMULATION AND PERFORMANCE ANALYSIS

A. SIMULATION SETTING

To verify the closed-loop control allocation performance, dynamic inversion theory is used to design the attitude angle control law subsystem and calculate the desired moment coefficients for control allocation. The control system architecture is shown in Fig 11, and the dynamic inversion method is described in **APPENDIX**.

Taking attitude tracking during cruising as an example, the allocation performance is ranked in order of importance:

* **Priority 1:** minimize allocation error J_0;
* **Priority 2:** minimum energy cost of actuators J_1, minimum drag coefficient J_3;
* **Priority 3:** maximum lift coefficient J_2.

The simulation parameter settings are as follows:

- **Attitude angel command:**
  - The roll and pitch angle commands ϕ_{des}, θ_{des} are square wave signals ranging from -5° to 5°;
  - The yaw angle commands ψ_{des} is a constant of 0.
- **Initial conditions:**
  - aerodynamic angle $[\alpha_0, \beta_0] = [2.3°, 0°]$;

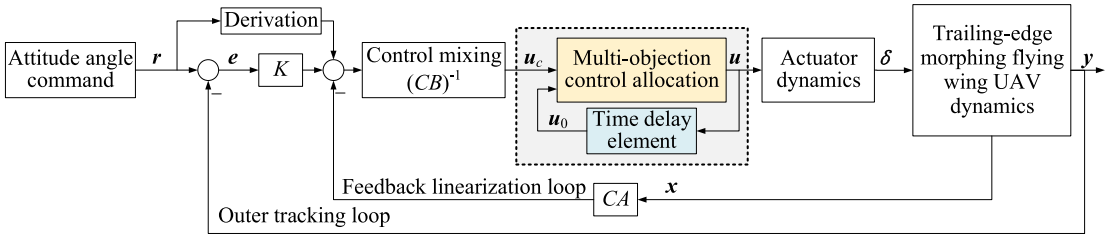

FIGURE 11. Attitude angle tracking flight control system.

Algorithm 1 Pseudocode for the H-MOPSO Algorithm

Input: $\mathbf{v}(t)$, $\mathbf{u}_0$, α, β, Ma and the Kriging aerodynamic model

Output: $\mathbf{U}$

Initialization n, $i_{\max}$, $w_{\min}$, $w_{\max}$, c_1 and c_2.

Step 1: Generate a random initial population of n individuals $\mathbf{U}_0$

Step 2: Evaluate the multiple objective function fitness values $J_0, \cdots, J_3$

Step 3: Choose the initial $\mathbf{P}_{\text{best\_0}}$ and $\mathbf{G}_{\text{best\_0}}$. $\mathbf{P}_{\text{best}} \leftarrow \mathbf{P}_{\text{best\_0}}$, $\mathbf{G}_{\text{best}} \leftarrow \mathbf{G}_{\text{best\_0}}$.

Step 4:

while the stopping criterion is not satisfied **do**

  for $i = 1$ to n **do**

    Step 4.1: Update velocity and position

    Step 4.2: Evaluate the multiple objective function fitness values $J_0, \cdots, J_3$,

    Step 4.3: Choose the $\mathbf{P}_{\text{best\_}i}$ and $\mathbf{G}_{\text{best\_}i}$.

  end for

  Step 4.4: Update

  Choose the optimal individual $\mathbf{P}_{\text{best}} \leftarrow \mathbf{P}_{\text{best\_}i}$, $\mathbf{G}_{\text{best}} \leftarrow \mathbf{G}_{\text{best\_}i}$.

end while

Return

  - Altitude angel $[\phi_0, \theta_0, \psi_0] = [0°, 2.3°, 0°]$;
  - Angular rate $[p_0, q_0, r_0] = [0°, 0°, 0°]$;
  - Flight speed, wind speed and altitude $[V_0, V_{w0}, H_0] =$ [50m/s, 0m/s, 1000m].

- **Time setting**
  - Sampling time: 0.05 s;
  - Simulation duration: 20 s.

B. SIMULATION RESULTS AND ANALYSIS

To validate the effectiveness of our proposed multi-objective control allocation method, we carry out flight simulations based on the H-MOPSO and C-MOPSO methods under the same simulation conditions. We compare the simulation results from the following aspects.

1) ATTITUDE ANGLE TRACKING RESULTS

First, the attitude angle (including the roll angle ϕ, pitch angle θ and yaw angle ψ) tracking results are compared, as shown in Fig. 12 to Fig. 14.

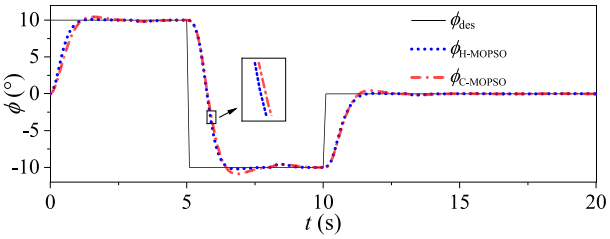

FIGURE 12. Tracking results of roll angle.

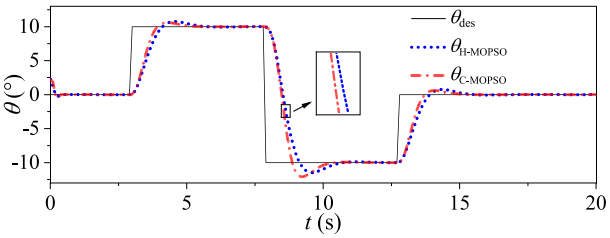

FIGURE 13. Tracking results of pitch angle.

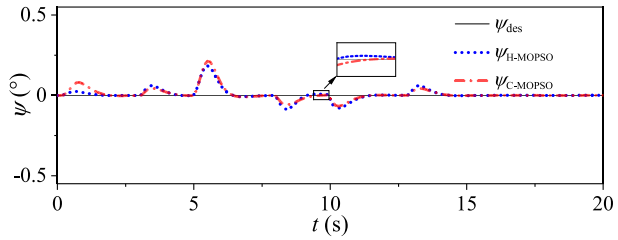

FIGURE 14. Tracking results of yaw angle.

From the attitude angle tracking results in Fig. 12 to Fig. 14, it can be seen that the two methods have similar tracking performances.

- For the roll angle tracking performance, the transition time (steady-state tracking error less than 5%) is less than 1.85s and the maximum overshoot is 2.2% for the H-MOPSO, and for C-MOPSO algorithm, the corresponding values are 2.60s and 8.8%.
- For the pitch angle tracking performance, the transition time (steady-state tracking error less than 5%) is less than 2.40 s and the maximum overshoot is 14.8% for H-MOPSO, and for C-MOPSO algorithm, the corresponding values are 2.10 s and 20.3%.
- For the yaw angle tracking performance, the maximum tracking errors are 0.18°(H-MOPSO) and 0.21°(C-MOPSO) at 1.25 seconds.

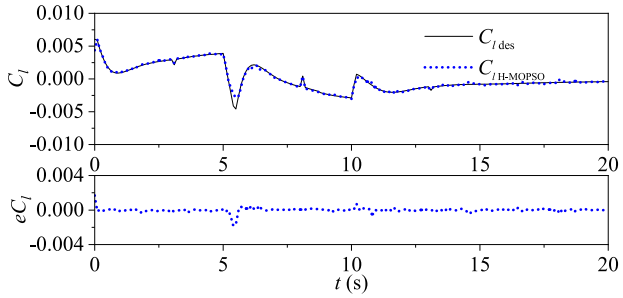

(a) Control allocation results of C_l based on H-MOPSO

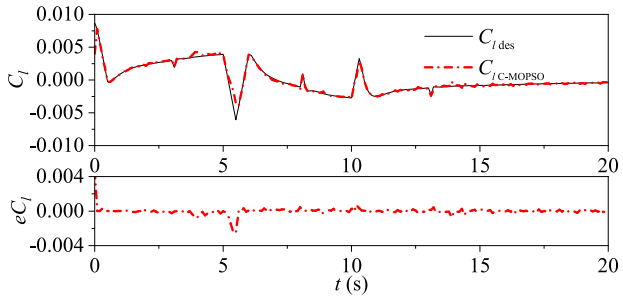

(b) Control allocation results of C_l based on C-MOPSO

FIGURE 15. Allocation results of roll moment coefficient.

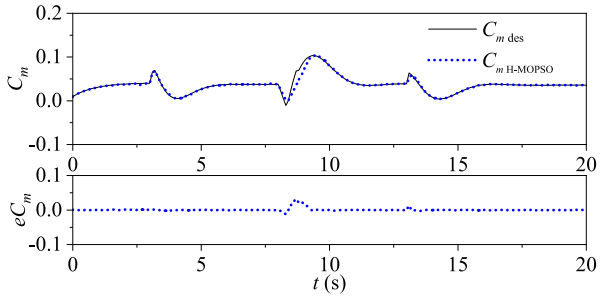

(a) Control allocation results of C_m based on H-MOPSO

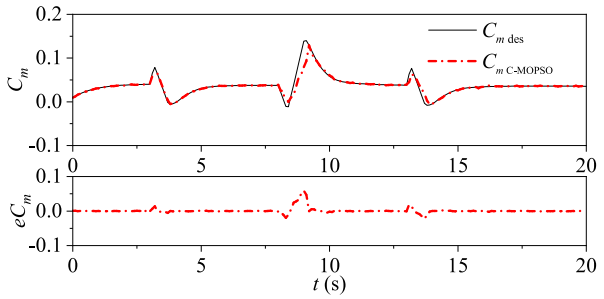

(b) Control allocation results of C_m based on C-MOPSO

FIGURE 16. Allocation results of pitch moment coefficient.

These results indicate that both the C-MOPSO method and H-MOPSO method can well meet the performance requirements for attitude angle tracking. Since both C-MOPSO and H-MOPSO methods take the allocation error (J0) as the primary optimization objective, the results obtained by the two methods have little difference in allocation error. Therefore, they have similar performance in the tracking errors.

2) ALLOCATION ERROR

The control allocation results of the triaxial moment coefficients are shown in Fig.15 to Fig.17.

As seen in the desired moment tracking curves in Fig. 15 to Fig. 17, both methods can track the desired moment coefficients well, and the maximum allocation error occurs when the control commands change. It can be seen in Fig. 12 to Fig. 17 that the control allocation method based on H-MOPSO and the method based on C-MOPSO have nearly similar characteristics in tracking performance and allocation errors because both control allocation methods take allocation errors as the most important optimization objective. Although there are some differences in the allocation errors between the two methods, the attitude angle tracking results of the two methods show almost the same performance due to the robustness of the feedback control law.

3) ENERGY COST OF ACTUATOR DEFLECTIONS

For the deflection angle of each actuator, the comparison results of the two methods are shown in Fig. 18, and the energy cost of actuator deflections E is shown in Fig. 19, where $E(t) = ||\mathbf{u}(t) - \mathbf{u}_0||$, $\mathbf{u} = [\delta_{\mathrm{L1}}, \delta_{\mathrm{L2}}, \cdots, \delta_{\mathrm{R4}}]^{\mathrm{T}}$.

By comparing the actuator deflection angles of the two methods, it can be found that the deflection angle obtained by

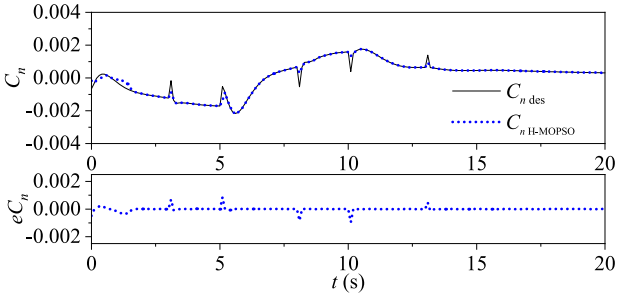

(a) Control allocation results of C_n based on H-MOPSO

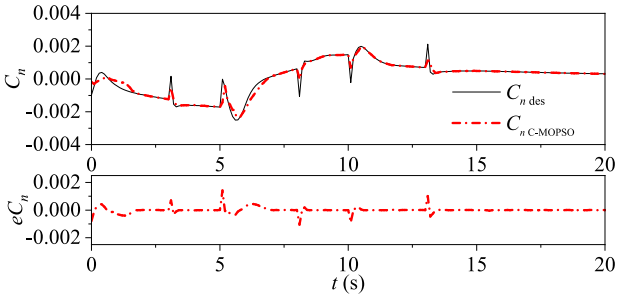

(b) Control allocation results of C_n based on C-MOPSO

FIGURE 17. Allocation results of the yaw moment coefficient.

H-MOPSO is smoother and the peak value is relatively small. Regarding the energy cost in Fig. 19, the average energy cost E_{avg} of H-MOPSO is 1.32, while that of C-MOPSO is 1.73.

4) C_D AND C_L

The drag coefficient C_D and the lift coefficient C_L are shown in Fig. 20 and Fig. 21. Compared with the C-MOPSO method, the drag coefficient is reduced by 4.43%, and the lift coefficient is increased by 2.23%.

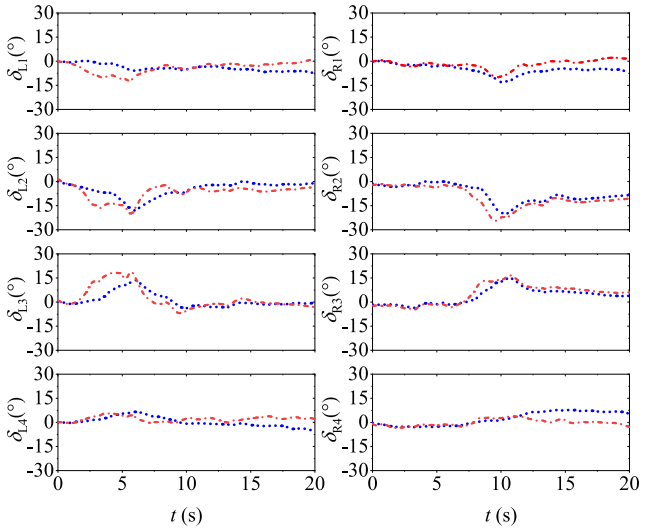

FIGURE 18. Actuator deflections.

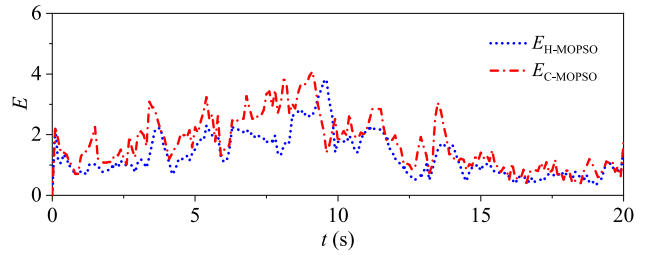

FIGURE 19. Energy cost of actuator deflections.

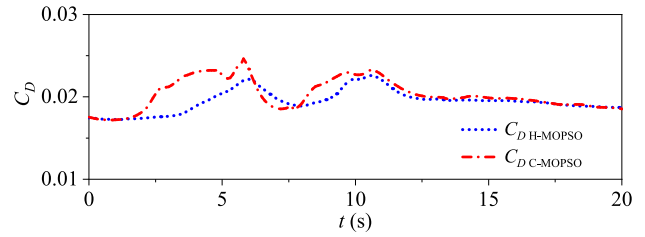

FIGURE 20. Drag coefficient.

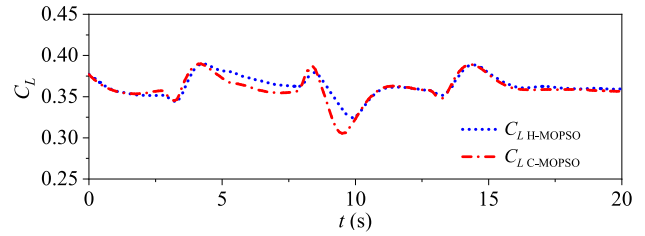

FIGURE 21. Lift coefficient.

Finally, Table. 4 lists the maximum allocation errors ($eC_{x\text{–max}}$; from top to bottom, they are $eC_{l\text{–max}}$, $eC_{m\text{–max}}$ and $eC_{n\text{–max}}$, respectively), the energy cost of the actuator (E_{avg}), the lift coefficient ($C_{L\text{–avg}}$) and the drag coefficient ($C_{D\text{–avg}}$) of the two methods.

It can be seen in Fig. 12 to Fig. 21 and Table. 4 that control allocation methods based on H-MOPSO and C-MOPSO have similar performance in attitude angle tracking, while the other

TABLE 4. Performance comparison of control allocation methods based on H-MOPSO and C-MOPSO.

Method	$eC_{x\text{–max}}$	E_{avg}	$C_{D\text{–avg}}$	$C_{L\text{–avg}}$
H-MOPSO	1.69×10^{-3} 3.28×10^{-2} 8.44×10^{-4}	1.32	0.0194	0.366
C-MOPSO	4.65×10^{-3} 5.98×10^{-2} 1.42×10^{-3}	1.73	0.0203	0.358
Comparison	-	-23.70%	-4.43%	+2.23%

performances of the H-MOPSO method are improved (the energy cost is reduced by 23.70%, the drag is reduced by 4.43% and the lift is increased by 2.23%).

VI. CONCLUSION

In this paper, we designed a continuous morphing trailing-edge for a flying wing UAV, replacing traditional discrete control surfaces. Different from conventional control allocation methods, we presented a nonlinear -multi-objective control allocation method based on the Kriging aerodynamic model, which can handle the nonlinear and coupling characteristics of the morphing control surface. More explicitly, to build the Kriging model efficiently, the non-uniform optimal LHS method is applied to generate initial sample points, and the MSE infill-sampling criterion is used to generate new samples. Based on the Kriging aerodynamic model, we proposed two algorithms to solve the control allocation problem: C-MOPSO and H-MOPSO. Simulation results show that both the C-MOPSO and H-MOPSO methods can suitably satisfy the performance requirements for attitude angle tracking, while the H-MOPSO method can achieve better multi-objective allocation performance.

To improve the accuracy of aerodynamic modeling and to further reduce the control allocation error, it is good direction to focus on the multi-fidelity aerodynamic surrogate modeling. Additionally, how to improve the calculation speed of multi-objective optimization also deserves further research.

APPENDIX. DYNAMIC INVERSION CONTROL LAW

Dynamic inversion is used to design the attitude angle control subsystem and calculate the desired moment coefficients. Dynamic inversion method, also refers to feedback linearization, is a control strategy that uses the model of itself to control the system, thereby eliminates the gain scheduling requirements and improves system performance. The dynamic equation of morphing trailing-edge UAVs can be described in state-variable form by

$$\begin{cases} \dot{\boldsymbol{x}} = A\mathbf{x} + B\mathbf{u_c} \\ \mathbf{y} = C\mathbf{x}, \end{cases} \tag{22}$$

where state $\mathbf{x} = [V, \alpha, \beta, p, q, r, \phi, \theta, \psi]^{\mathrm{T}}$, virtual control input $\mathbf{u_c} = [C_{l\ \text{des}}, C_{m\ \text{des}}, C_{n\ \text{des}}]^{\mathrm{T}}$, and control output $\mathbf{y} = [\phi, \theta, \psi]^{\mathrm{T}}$. A, B and C are the system matrix, the input matrix and the output matrix, respectively. The entire state $\mathbf{x}$ is available for feedback purposes.

The number of inputs is equal to the number of outputs so that the system is square. A square system is desired to control the output $\mathbf{y}(t)$ so that it follows a desired attitude angle reference trajectory $\mathbf{r} = [\phi_{\text{des}}, \theta_{\text{des}}, \psi_{\text{des}}]^{\text{T}}$. Define the tracking errors as

$$\mathbf{e}(t) = \mathbf{r}(t) - \mathbf{y}(t). \tag{23}$$

The simple dynamic inversion control input is given by

$$\mathbf{u_c} = (CB)^{-1}(\dot{\mathbf{r}} + K\mathbf{e} - CA\mathbf{x}), \tag{24}$$

where K is usually a positive diagonal matrix to keep the control channels in the outer loop decoupled. More details on the dynamic inverse controller and UAV modeling can be found in [25].

REFERENCES

[1] M. Tomac and G. Stenfelt, "Predictions of stability and control for a flying wing," *Aerosp. Sci. Technol.*, vol. 39, pp. 179–186, Dec. 2014.
[2] M. Li, J. Bai, L. Li, X. Meng, Q. Liu, and B. Chen, "A gradient-based aero-stealth optimization design method for flying wing aircraft," *Aerosp. Sci. Technol.*, vol. 92, pp. 156–169, Sep. 2019.
[3] R. H. Liebeck, "Design of the blended wing body subsonic transport," *J. Aircr.*, vol. 41, no. 1, pp. 10–25, Jan. 2004.
[4] P. Okonkwo and H. Smith, "Review of evolving trends in blended wing body aircraft design," *Prog. Aerosp. Sci.*, vol. 82, pp. 1–23, Apr. 2016.
[5] D. Li, S. Zhao, A. D. Ronch, J. Xiang, J. Drofelnik, Y. Li, L. Zhang, Y. Wu, M. Kintscher, H. P. Monner, A. Rudenko, S. Guo, W. Yin, J. Kirn, S. Storm, and R. D. Breuker, "A review of modelling and analysis of morphing wings," *Prog. Aerosp. Sci.*, vol. 100, pp. 46–62, Jun. 2018.
[6] Z. Yao and S. Wu, "Intermittent gliding flight control design and verification of a morphing unmanned aerial vehicle," *IEEE Access*, vol. 7, pp. 40991–41005, 2019.
[7] Q. Wang, L. Gong, C. Dong, and K. Zhong, "Morphing aircraft control based on switched nonlinear systems and adaptive dynamic programming," *Aerosp. Sci. Technol.*, vol. 93, pp. 1–16, Oct. 2019.
[8] D. Keidel, U. Fasel, and P. Ermanni, "Control authority of a camber morphing flying wing," *J. Aircr.*, vol. 57, no. 4, pp. 603–614, Jul. 2020.
[9] T. A. Johansen and T. I. Fossen, "Control allocation: A survey," *Automatica*, vol. 49, no. 5, pp. 1087–1103, 2013.
[10] V. L. Poonamallee, S. Yurkovich, A. Serrani, and D. B. Doman, "A nonlinear programming approach for control allocation," in *Proc. Amer. Control Conf.*, vol. 2, 2004, pp. 1689–1694.
[11] D. Doman and M. Oppenheimer, "Improving control allocation accuracy for nonlinear aircraft dynamics," in *Proc. AIAA Guid., Navigat., Control Conf. Exhibit*, Aug. 2002, pp. 1–10.
[12] M. A. Bolender and D. B. Doman, "Nonlinear control allocation using piecewise linear functions," *J. Guid., Control, Dyn.*, vol. 27, no. 6, pp. 1017–1027, Nov. 2004.
[13] G. G. Wang and S. Shan, "Review of metamodeling techniques in support of engineering design optimization," in *Proc. Int. Design Eng. Tech. Conf. Comput. Inf. Eng. Conf.*, vol. 4255, Jan. 2006, pp. 415–426.
[14] S. Koziel and A. Pietrenko-Dabrowska, "Rapid optimization of compact microwave passives using Kriging surrogates and iterative correction," *IEEE Access*, vol. 8, pp. 53587–53594, 2020.
[15] X. Chai, Z. Sun, J. Wang, Y. Zhang, and Z. Yu, "A new Kriging-based learning function for reliability analysis and its application to fatigue crack reliability," *IEEE Access*, vol. 7, pp. 122811–122819, 2019.
[16] Q. Liu and G. Jiao, "A pipe routing method considering vibration for aero-engine using Kriging model and NSGA-II," *IEEE Access*, vol. 6, pp. 6286–6292, 2018.
[17] K. R. Olympio and F. Gandhi, "Flexible skins for morphing aircraft using cellular honeycomb cores," *J. Intell. Mater. Syst. Struct.*, vol. 21, no. 17, pp. 1719–1735, Nov. 2010.
[18] A. Dean, D. Voss, and D. Draguljić, *Design and Analysis of Experiments*, vol. 1. Springer, 2017.
[19] H. Kaya, H. Tiftikçi, U. Kutluay, and E. Sakarya, "Generation of surrogate-based aerodynamic model of an UCAV configuration using an adaptive co-Kriging method," *Aerosp. Sci. Technol.*, vol. 95, pp. 1–8, Dec. 2019.
[20] J. P. C. Kleijnen, "Regression and Kriging metamodels with their experimental designs in simulation: A review," *Eur. J. Oper. Res.*, vol. 256, no. 1, pp. 1–16, Jan. 2017.
[21] D. Zhan and H. Xing, "Expected improvement for expensive optimization: A review," *J. Global Optim.*, vol. 78, no. 3, pp. 507–544, Nov. 2020.
[22] D. Liu, J. Wu, K. Lin, and M. Wu, "Planning of multi energy-type micro energy grid based on improved Kriging model," *IEEE Access*, vol. 7, pp. 14569–14580, 2019.
[23] V. R. Kulkarni and V. Desai, "ABC and PSO: A comparative analysis," in *Proc. IEEE Int. Conf. Comput. Intell. Comput. Res. (ICCIC)*, Dec. 2016, pp. 1–7.
[24] L. Sun, Q. Zhou, B. Jia, W. Tan, and H. Li, "Effective control allocation using hierarchical multi-objective optimization for multi-phase flight," *Chin. J. Aeronaut.*, vol. 33, no. 7, pp. 2002–2013, Jul. 2020.
[25] B. L. Stevens, F. L. Lewis, and E. N. Johnson, *Aircraft Control and Simulation: Dynamics, Controls Design, and Autonomous Systems*. Hoboken, NJ, USA: Wiley, 2015.

XINHUI ZHAO received the M.S. degree in mechanical engineering from the China University of Petroleum, in 2018. He is currently pursuing the Ph.D. degree in flight vehicle design with the Institute of Engineering Thermophysics, Chinese Academy of Sciences, Beijing, China.

He is also investigating the project fault-tolerant flight control system of flying wing UAV. His research interests include the UAV systems and flight control law design. He also serves as a Reviewer of the IEEE WCSP 2019.

YANPING YANG received the B.S. degree in automation and the M.S. degree in electronics engineering from Xidian University, Xi'an, China, in 2008 and 2013, respectively, and the Ph.D. degree from the National Digital Switching System Engineering and Technological Research and Development Center, Zhengzhou, China.

He studied at the Department of Electronic Engineering, Tsinghua University. He is currently holding a postdoctoral position at the Institute of Engineering Thermophysics, Chinese Academy of Sciences, Beijing, China. He has published more than 20 articles around his research directions, including IEEE TRANSACTIONS ON COMMUNICATIONS (IEEE TCOM), IEEE TRANSACTIONS ON VEHICULAR TECHNOLOGY (IEEE TVT), and IEEE ACCESS. His research interests include UAV formation flight, UAV systems, flight control law design, wireless communications, cognitive radio networks, and network coding. He also serves as TPC of IEEE WCSP 2019. He also serves a Reviewer of the IEEE JOURNAL ON SELECTED AREAS IN COMMUNICATIONS (IEEE JSAC), IEEE TRANSACTIONS ON COMMUNICATIONS, IEEE TRANSACTIONS ON VEHICULAR TECHNOLOGY, ICC, and GlobeCom.

XIAOPING MA received the bachelor's, master's, and Ph.D. degrees in aircraft design from Northwestern Polytechnical University, in 1983, 1988, and 2008, respectively.

He has been engaged in the research and development of UAV system for a long time. He has participated in various types of UAV, working as the Deputy Chief Engineer and Chief Engineer. He has published more than 20 articles that related to UAV designs, among which five were retrieved by EI/SCI/ISTP/SSCI. His main research interests include the UAV systems, the aircraft and structure design, launching and recovering technique, and system flight test. He also serves as a Senior Member of the Aviation Society of China. He has received the first prize and the second prize of the National Science and Technology Progress, the second prize of National Commission of Science, Technology and Industry for National Defense, the first prize and the second prize of Ministerial Awards.